

# Role of MgO Buffer Layer on Defect Reduction of P-MBE Grown ZnO Layer on c-sapphire

A. Setiawan<sup>1</sup>, M. W. Cho<sup>2</sup>, and T. Yao<sup>2</sup>

<sup>1</sup> Department of Mechanical Engineering, Indonesia University of Education  
Setiabudhi 229 Bandung 40154, Indonesia

<sup>2</sup> Center for Interdisciplinary Research, Tohoku University  
Aramaki, Aoba-ku, Sendai, 980-8578, Japan

## Abstract

We have investigated the role of low temperature (LT)-MgO buffer layers on defect reduction of ZnO layers grown on c-sapphire by plasma-assisted molecular beam epitaxy (P-MBE). Buffer growth parameters consisting of thickness, growth rate, and annealing were evaluated. We found that surface morphology and crystalline quality of the ZnO layers were improved by controlling the buffer layers. There is no improvement in morphology and crystalline quality of the ZnO layers if the buffer thickness is less than critical thickness. The critical thickness of MgO buffer is determined to be 1.5 nm. We also found that low growth rate of the buffer layers is preferred for high quality ZnO layer. Furthermore, surface, structural, optical, and electrical qualities of the ZnO layers were improved by annealing MgO buffer at high temperature. Dislocation density of the ZnO layer was reduced from  $5.3 \times 10^9 \text{ cm}^{-2}$  to  $1.9 \times 10^9 \text{ cm}^{-2}$  by annealing the MgO buffer layer. The results indicate that we can engineer defect in highly mismatched heteroepitaxial using buffer layers.

**Keywords** : ZnO, MgO, Plasma-assisted MBE.

## I. Introduction

ZnO is a direct band gap semiconductor ( $E_g=3.37 \text{ eV}$  at RT) with a wurtzite structure. The most unique property of ZnO is its large exciton binding energy, 60 meV, which is about three times larger than that of ZnSe or GaN. Recent reports on the lasing mechanisms of ZnO have shown that ZnO is a promising photonic material for exciton devices in the wavelengths ranging from blue to ultraviolet[1-3].

High quality ZnO is a prerequisite for ZnO-based optical device applications. At present, challenges of moving toward device applications are the difficulty in achieving high crystal quality in either bulk or thin film dimensions of ZnO, as well as the difficulty in controlling p-type conductivity. On the other hand, controlling the crystalline defects in naturally n-type ZnO is the critical issue to obtain p-type ZnO.

Low price high quality c-sapphire ( $\alpha\text{-Al}_2\text{O}_3$ ) has been extensively used as a substrate for ZnO epitaxy in many growth techniques, including chemical vapor deposition [4-6], pulsed laser deposition,<sup>7,8</sup> and P-MBE [9,10]. Among these growth techniques, P-MBE has shown high controllability to grow high crystal-quality ZnO layers. Because of the large lattice misfit between ZnO and c-sapphire (18%) and the formation of  $30^\circ$  rotated domains [11] ZnO layers grown on c-

sapphire showed rough surface morphology and poor crystalline quality [9-11].

In order to overcome the problems caused by the large mismatch between ZnO and c-sapphire substrate, the growth of double buffer layers consisting of low temperature (LT)-MgO buffer and LT-ZnO buffer followed by high temperature annealing has been utilized with success by P-MBE [12,13]. Consequently, the growth of high temperature (HT) ZnO is dominated by layer-by-layer growth, the formation of  $30^\circ$ -rotated domains is completely suppressed, and the dislocation density is reduced. However, the dislocation density still remains high, in particularly edge dislocation [14]. Therefore, further reducing of the ZnO dislocation density is crucial for device applications.

The use of a buffer layer is the most widespread technique used in heteroepitaxy. The residual strain caused by the uncompleted relaxation in the buffer layer can generate additional defects during subsequent growth and there will be a relatively high density of threading dislocations (TDs) extended to the device region. Therefore, buffer growth parameters such as thickness, growth temperature, and growth rate should be precisely controlled. The thickness and annealing of buffer layer influence the strain situation, while the growth rate and growth temperature influence the wetting process. Furthermore, annealing of a LT-buffer layer make

the flattening process more fast because the migration on the surface is enhanced during growth interruption and at high temperature [14]. At present, there are no detailed studies on the control of the growth of MgO buffer layers in ZnO P-MBE on c-sapphire. In the present paper we report the role of MgO buffer layers on defect reduction of the ZnO layers.

## II. Experiment

The c-sapphire substrate was degreased in acetone and methanol in an ultrasonic cleaner followed by rinsing in deionized water. The substrate was then chemically etched in a  $\text{H}_2\text{SO}_4$  (96%):  $\text{H}_3\text{PO}_4$  (85%) = 3:1 solution. Prior to growth, the substrate was thermally cleaned at 750 °C in the preparation chamber for 1 hour. The substrate was then treated in oxygen plasma at 650 °C for 30 minutes in the growth chamber to produce an oxygen terminated c-sapphire surface. The sample structure is ZnO/ZnO-buffer/MgO-buffer/c-sapphire. What we have done in this research is effects of LT-MgO buffer thickness and its annealing on the quality of ZnO layers. The buffer layers were grown under optimum growth temperature; at 490 °C for MgO buffer and 500 °C for ZnO buffer. ZnO buffer was annealed at 750 °C for 5 minutes. High temperature ZnO layers were grown at 700 °C. In the case of ZnO layers grown with MgO buffer annealing, the MgO buffer was annealed at 800 °C for 25 minutes. ZnO layers were then characterized by Atomic force microscopy (AFM), high resolution x-ray diffraction (HRXRD), cross-sectional transmission electron microscopy (TEM), Photoluminescence (PL), and Hall measurement. HRXRD experiments were carried out with a Phillips X'Pert MRD diffractometer. Cross sectional TEM experiments were carried out with a JEOL JEM 2000 EX II operated at 200 kV.

## III. Results and Discussion

### A. LT-MgO buffer thickness

First, we discuss effect of MgO buffer thickness on the surface morphology and crystalline quality of ZnO layer. Figure 1 shows RHEED pattern and AFM image of ZnO layers grown on c-sapphire under different LT-MgO buffer thicknesses. Based on in-situ RHEED observation, the growth of MgO buffer involves three important steps including wetting layer MgO (~ 0.5 nm thick), 2D-3D growth transition (~1.5 nm thick), and 3D growth MgO (~3 nm thick) [12]. ZnO layer grown on wetting layer MgO shows 3D growth, as indicated by spotty RHEED

pattern and 3D island growth with root mean square (rms) value of surface roughness as large as 19.9 nm. In contrast, ZnO layers grown on MgO buffer after 2D-3D growth transition show 2D growth, as indicated by streaky RHEED pattern and layer-by-layer growth with rms value of roughness lower than 1 nm.

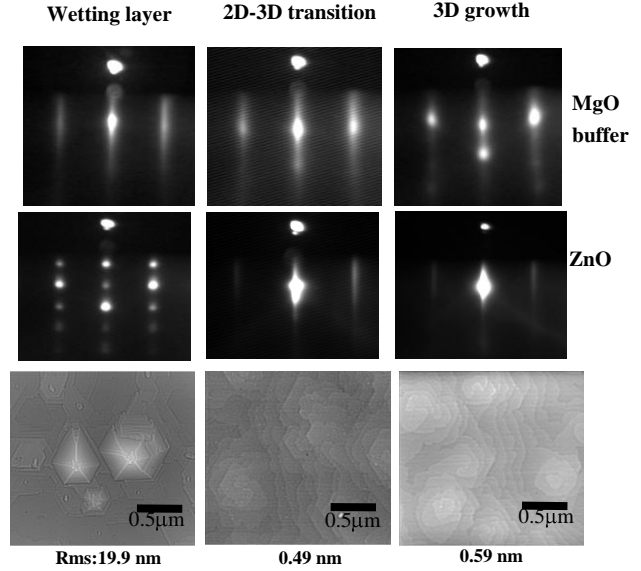


**Fig. 1.** RHEED patterns and AFM images of ZnO P-MBE on c-sapphire with different MgO buffer thicknesses (growth stage).

Now let us discuss the role of buffer layers on defect reduction of the ZnO layers. Table 1 provides a comparison of characteristics of ZnO layers grown on c-sapphire without MgO buffer and with various MgO buffer thicknesses.

**Table 1.** Characteristics of ZnO layers grown on c-sapphire without and with various MgO buffer thicknesses.

ZnO grown on	AFM Growth Mode	AFM surface roughness in 2.5 μm x 2.5 μm (nm)	FWHM of rocking curves (arcsec)	
			(0002)	(10-11)
c-sapphire	3D	41.0	566	1346
Wetting layer MgO (< 1 nm)	3D	19.9	640	1897
2D-3D transition (~1.5 nm)	2D	0.49	12	1033
3D grown MgO (~3 nm)	3D	0.59	16	990

ZnO grown on c-sapphire was characterized by 3D growth with rough surface morphology and poor crystalline quality as indicated by large full width at half maximum (FWHM) values of (0002)  $\Omega$  and (10-11) $\Omega$  rocking curves. In the case of employing MgO buffer layer, no improvement in morphology and crystal quality can be obtained if ZnO is grown directly on the MgO wetting layer before the 2D-3D transition occurs as indicated by 3D growth with high rms value of roughness and large FWHM value of the (0002)  $\Omega$  and (10-11)  $\Omega$  rocking curves. In order to explain this case, Fig.2 shows in-situ RHEED observation of in-plane lattice constant versus MgO buffer thickness. The MgO buffer thickness is determined by multiplication of MgO buffer growth rate and growth time.

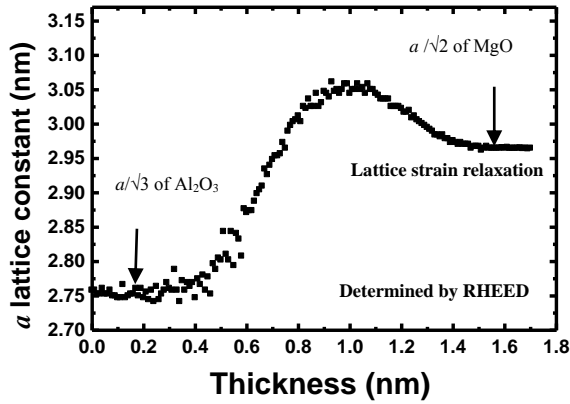


Fig. 2. In-situ RHEED observation of in-plane lattice constant versus MgO buffer thickness.

As shown in Fig. 2, the lattice constant changes with increasing MgO buffer thickness and saturates after around 1.5 nm thick. Saturation point implies a complete lattice strain relaxation. When ZnO layer is grown on wetting layer MgO with around 0.5 nm thick, the lattice is not completely relaxed yet. Consequently, there is no improvement in ZnO crystalline quality as indicated by the large FWHM value of  $\Omega$  rocking curves. In contrast, when ZnO is grown on MgO buffer after 2D-3D growth transition, in which the thickness is much thicker than 1.5 nm, the strain is already completely relaxed. Relaxation of strain in MgO buffer contributes to the lowering of surface energy, leading to improvement of ZnO layer. Furthermore, the 2D-3D transition resulted in islands that provide nucleation sites and facilitate the following ZnO growth. In addition, the slip system in rocksalt structure MgO is  $1/2\langle 110 \rangle\{110\}$  [15] and the MgO buffer was grown along [111] direction [14]. Therefore, the most favorable dislocation direction in MgO is not

along the  $c$ -axis. Consequently, interaction between dislocations might be introduced when ZnO initially nucleates on a faulty MgO islands layer rather than on perfect c-sapphire. Here we should note here that employing MgO buffer layer improved surface morphology and crystalline quality of the ZnO layers.

### B. Annealing of LT-MgO buffer layer

Let us discuss effect of LT-MgO buffer annealing on the quality of ZnO layer. Figure 3 shows AFM images of a LT-MgO buffer (a) and a LT-MgO buffer annealed at 800 C for 25 minutes (b). Images of a ZnO layer grown on LT-MgO buffer and on an annealed LT-MgO are shown in (c) and (d), respectively. Comparison of the images (a) and (b) clearly shows that surface morphology of the MgO buffer is greatly improved by annealing, as indicated by the reduced surface roughness of MgO from 2.7 nm to 0.2 nm. Furthermore, surface roughness of the ZnO layers are 0.6 nm and 0.3 nm, for (c) and (d), respectively, while step height (terraces size) average 0.2 nm (94 nm) and 0.3 nm (245 nm) for (c) and (d), respectively. Here we note that annealing LT-MgO buffer at high temperature enhanced the surface migration of adatoms, leading to the formation of larger terraces on the surface and smoother surface morphology of ZnO layer.

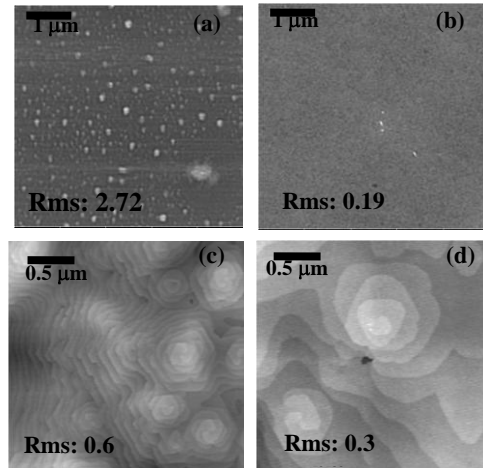
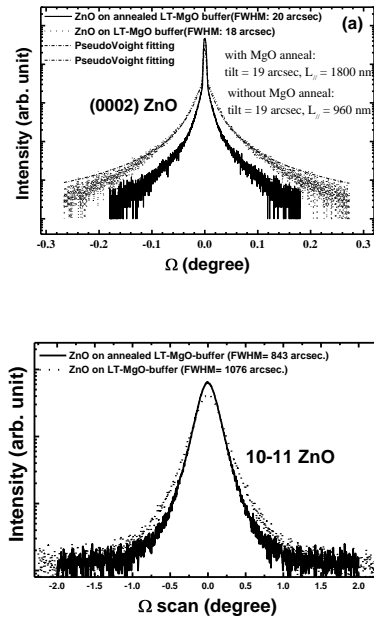


Fig. 3. AFM images of (a) LT-MgO buffer and (b) LT-MgO buffer annealed at 800 °C for 25 minutes. Images (c) and (d) show corresponding images of ZnO layers grown on a LT-MgO buffer layer and on an annealed LT-MgO buffer, respectively

Crystalline quality of ZnO layers were addressed by HRXRD. Figure 4 shows (a) (0002)  $\Omega$  and (b) (10-11)  $\Omega$  rocking curves for ZnO layers

grown on a LT-MgO buffer and on an annealed LT-MgO buffer. FWHM values of (0002) $\Omega$  rocking curves (in arcsec) are 18(1076) and 22(843), respectively for ZnO layers grown on a LT-MgO buffer and on an annealed LT-MgO buffer. Nearly the same low FWHM values of (0002) $\Omega$  scans for these two samples imply low screw dislocation density in both. However, the line shape of (0002) reflection for ZnO layer grown with MgO buffer annealing has a more Gaussian shape and narrow tail compared to ZnO layer grown without MgO annealing. These features are an indication of the improvement of the interface region by MgO buffer annealing. A much broader (10-11)  $\Omega$  reflection than (0002) reflection implies the present of a high density of edge-type dislocations. Note that all types of dislocations (edge, screw, and mixed) broaden the (10-11) reflection, whereas the (0002) reflection is only sensitive to screw and mixed type dislocations [16,17]. Furthermore, the FWHM values of the (10-11)  $\Omega$  scan of the ZnO layer grown on annealed MgO buffer is smaller than that grown on a LT-MgO buffer, indicating much lower edge dislocation density.



**Fig. 4.** (a) (0002)  $\Omega$  and (b) (10-11)  $\Omega$  rocking curves of ZnO layers grown on LT-MgO buffer layer (dotted curve) and grown on annealed LT-MgO buffer (solid curve).

It is interesting to correlate the surface morphology addressed by AFM and grain size or lateral coherence length ( $L_{//}$ ) addressed by HRXRD. In order to determine  $L_{//}$ , the line shape of (0002)  $\Omega$  scans was fitted by Pseudo-Voigt

function which will give information about tilt angle ( $\alpha_{\Omega}$ ) and  $L_{//}$ . Details of this procedure are given in Ref. [18]. The fitting revealed the value of  $\alpha_{\Omega}$  ( $L_{//}$ ) are 19 arcsec (1800 nm) and 19 arcsec (960 nm), for ZnO layers grown with and without LT-MgO buffer annealing, respectively. Here, the grain size of ZnO layer was increased by almost twice by annealing of the LT-MgO buffer layer. HRXRD and AFM data show that annealing of MgO buffer increased the grain size and terrace size, leading to a lowering rms value of surface roughness from 0.6 to 0.3 nm, which is equivalent to 1 ML ZnO.

Dislocations in ZnO layer grown with and without LT-MgO buffer annealing was characterized by cross-sectional TEM under a two-beam condition as shown in Fig. 5. The samples were observed near the [2-1-10] zone axis with diffraction vectors  $\mathbf{g} = 0006$  [images (a) and (c)] and  $\mathbf{g} = 03-30$  [images (b) and (d)].

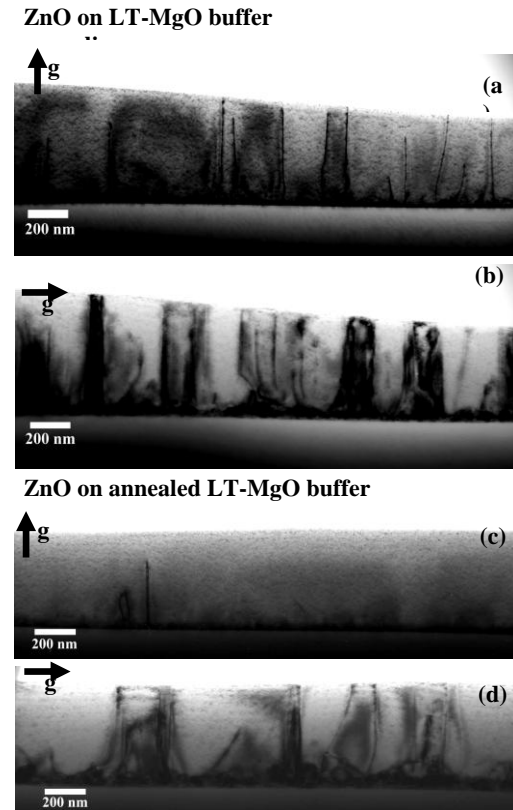


**Fig. 5.** Bright-field cross sectional electron micrographs of ZnO layers grown on LT-MgO buffer [images (a) and (b)] and grown on annealed LT-MgO buffer [images (c) and (d)]. The images were viewed along the [2-1-10] zone axis. The  $\mathbf{g} = 0006$  imaging conditions were used for (a) and (c) and  $\mathbf{g} = 03-30$  imaging conditions were used for (b) and (d).

In Fig.4, the predominantly extended defects are TDs parallel to the  $c$  axis, similar to the GaN films grown by MOCVD with a nitride layer [19] which are in contrast to the ZnO films grown directly on c-sapphire by pulsed laser deposition, for which stacking faults and dislocations lying in the basal plane were found to be the main extended defects [20]. Invisibility criterion,  $\mathbf{g}\cdot\mathbf{b} = 0$ , reveals that the images (a) and (c) show screw-component of dislocation, while the images (b) and (d) show edge-component of dislocations. After averaging several images for ZnO layer grown on LT-MgO buffer, TDs were distributed as 15% of screw-type (Burgers vectors of  $[0001]$ ), 67% of edge-type (Burgers vectors of  $1/3\langle 11-20 \rangle$ ), and 18% of mixed-type dislocations (Burgers vectors of  $1/3\langle 11-23 \rangle$ ). While for ZnO layers grown on an annealed MgO buffer threading dislocations were distributed as 90% of edge-type and 10% of screw-type dislocations. Because of extremely well lattice ordering in the growth direction as a result of well-controlled buffer layer, we did not observe mixed-type dislocation in the ZnO sample with MgO buffer annealing. The density of the edge dislocations is much higher than that of screw dislocations density in the both samples. It may be caused by the formation energy of a screw is larger than an edge dislocation by factor of 1.6 in ZnO [14,15]. Furthermore, only the edge type dislocation is able to accommodate the lattice mismatch strain, while the screw type dislocation forms much related to the initial nucleation environment. Total dislocation density was determined to be  $5.3 \times 10^9 \text{ cm}^{-2}$  and  $1.9 \times 10^9 \text{ cm}^{-2}$ , for the ZnO layers grown on LT-MgO and grown on annealed LT-MgO buffer, respectively. Here, dislocation density,  $D$ , was determined by formula  $D = n/lh$ , where  $n$  = number of dislocations,  $l$  = foil length, and  $h$  = foil thickness. The foil thickness was determined by measuring number of extinction distance fringes for two-beam,  $s = 0$ ,  $\mathbf{g} = 0002$ , images and using extinction distance as reference for the crystal thickness change with each fringe [21]. TEM results confirmed that the dislocation density of the ZnO layer was reduced by annealing of the LT-MgO buffer layers. These results are consistent with the HRXRD results as explained above.

At the interface region, highly faulted regions as well as basal dislocations located mainly on the basal plane were observed. However, the density rapidly decreases beyond 50 nm from the interface. This can only be understood if these dislocations are not along the  $c$ -axis so that they can strongly interact with each other and annihilate

quickly [14].

Table 2 provides a summary of properties of ZnO layer grown with and without MgO buffer annealing.

**Table 2.** Characteristics of ZnO layers grown with and without annealing of LT-MgO buffer.

Parameters	Without MgO annealing	With MgO annealing
Surface roughness (nm)	0.6	0.3
FWHM of (0002) $\Omega$ (arcsec)	18	20
FWHM of (10-11) $\Omega$ (arcsec)	1076	843
Dislocation density ( $\text{cm}^{-2}$ )	$5.3 \times 10^9$	$1.9 \times 10^9$
Intensity of free-exciton emission	Low	2x higher
Intensity of deep-level emission	High	1/3 lower
Electron mobility ( $\text{cm}^2/\text{V}\cdot\text{s}$ )	105	120
Carrier concentration ( $\text{cm}^{-3}$ )	$2.83 \times 10^{16}$	$1.71 \times 10^{17}$

As shown in Table 2, surface morphology of ZnO layer was improved by MgO buffer annealing as indicated by lower surface roughness and larger terrace width. Crystalline quality of ZnO layer was improved as indicated by lower dislocation density and FWHM value of (10-11)  $\Omega$  scan. Optical quality was also improved as indicated by higher intensity of free exciton emission and lower intensity of deep level emission. Electron mobility of ZnO was increased from 100 to 120  $\text{cm}^2/\text{V}\cdot\text{s}$  by annealing of MgO buffer layer. Therefore, annealing of MgO buffer layer at high temperatures improved surface morphology, structural, optical, and electrical quality of ZnO layer.

#### IV. Conclusions

We have investigated the role of LT-MgO buffer layers on defect reduction of ZnO P-MBE on c-sapphire. No improvement in morphology and crystalline quality of ZnO layer can be obtained if the buffer thickness is less than critical thickness. The critical thickness is determined to be 1.5 nm for MgO buffer. We found that low growth rate of the buffer layers is preferred for high quality ZnO layer. Furthermore, surface morphology, structural, optical, and electrical quality of the ZnO layer were improved by annealing MgO buffer at high temperature. Dislocation density of the ZnO layer was reduced from  $5.3 \times 10^9 \text{ cm}^{-2}$  to  $1.9 \times 10^9 \text{ cm}^{-2}$  by annealing the MgO buffer layer.

## V References

- 1 D. M. Bagnall, Y. F. Chen, Z. Zhu, T. Yao, S. Koyama, M. Y. Shen, T. Goto, Appl. Phys. Lett. **70**, 2230 (1997).
- 2 D.M. Bagnall, Y.F. Chen, Z. Zhu, T. Yao, M.Y. Shen, T. Goto, Appl. Phys. Lett. **73**, 1038 (1998).
- 3 H.J. Ko, Y.F. Chen, T. Yao, K. Miyajima, A. Yamamoto, T. Goto, Appl. Phys. Lett. **77**, 537 (2000).
- 4 S. Bethke, H. Pan, B. W. Wessels, Appl. Phys. Lett. **52**, 138 (1998).
- 5 T. Minami, H. Nanto, S. Tanaka, Jpn. J. Appl. Phys. **23**, 280 (1984).
- 6 K. Kobayashi, T. Matsubara, S. Matsushima, S. Shirakata, S. Isomura, G. Okata, Thin Solid Films **266**, 106 (1995).
- 7 S. Hayamizu, H. Tabata, H. Tanaka, T. Kawai, J. Appl. Phys. **80**, 787 (1996).
- 8 R. D. Vispute, V. Talyansky, Z. Trajanovic, S. Choopun, M. Downes, R. P. Sharma, M. C. Woods, R. T. Lareau, K. A. Jones, A. A. Iliadis, Appl. Phys. Lett. **70**, 2735 (1997).
- 9 M. A. L. Johnson, S. Fujita, W. H. Rowland, Jr., W.C. Hughes, J. W. Cook, Jr., J. F. Schetzina, J. Electron. Mater. **25**, 855 (1996).
- 10 Y. F. Chen, D. M. Bagnall, H. J. Ko, K. T. Park, K. Hiraga, Z. Zhu, T. Yao, J. Appl. Phys. **84**, 3912 (1998).
- 11 P. Fons, K. Iwata, A. Yamada, K. Matsubara, S. Niki, K. Nakahara, T. Tanabe, H. Takasu, Appl. Phys. Lett. **77**, 1801 (2000).
- 12 Y. F. Chen, H. J. Ko, S. K. Hong, T. Yao, Appl. Phys. Lett. **76**, 559 (2000).
- 13 Y. F. Chen, H. J. Ko, S. K. Hong, T. Yao, Y. Segawa, J. Cryst. Growth **214/215**, 87 (2000).
- 14 Y. F. Chen, S. K. Hong, H. J. Ko, V. Kirshner, H. Wenisch, T. Yao, K. Inaba, Y. Segawa, Appl. Phys. Lett. **78**, 3352 (2001).
- 15 J. P. Hirth, J. Lothe, *Theory of Dislocations*, 2nd Ed. John Wiley & Sons, New York, (1982).
- 16 B. Heying, X.H. Wu, S. Keller, Y. Li, D. Kapolnek, B. P. Keller, S.P. DenBaars, and J.S. Speck, Appl. Phys. Lett. **68**, 643 (1996).
- 17 Q. Zhu, A. Botchkarev, W. Kim, O. Aktas, A. Salvador, B. Sperdlov, H. Morkoc, S.C.Y. Tsen, and D. J. Smith, Appl. Phys. Lett. **68**, 9, 1141 (1996).
- 18 T. Metzger, R. Hopler, E. Born, O. Ambacher, M. Stutzmann, R. Stommer, M. Schuster, H. Gobel, S. Christiansen, M. Albrecht, and H.P. Strunk, Phil. Mag. A **77**, 1013 (1998).
- 19 F. A. Ponce, D. Cherns, W. T. Young, and J. W. Steeds, Appl. Phys. Lett. **69**, 770 (1996).
- 20 J. Narayan, K. Dovidenko, A. K. Sharma, and S. Oktyabrsky, J. Appl. Phys. **84**, 2597 (1998).
- 21 X. H. Wu, L. M. Brown, D. Kapolnek, S. Keller, B. Keller, S. P. DenBaars, and J. S. Speck, J. Appl. Phys. **80** (6), 3228 (1996).

## Acknowledgements

The author would like to thank Dr. H. J. Ko, Mr. Tsutomu Minegishi, Mr. Hiroki Goto, Mr. Chihiro Harada, and Mr. Takuma Suzuki for their help in experiments and discussions.